Supporting Information

Understanding Hydrazine Oxidation Electrocatalysis on Undoped Carbon

Tomer Y. Burshtein,[a] Kesha Tamakuala,[b] Nagaprasad R. Samala,[b] Matan Sananis,[a] Ilya Grinberg,[b] David Eisenberg[a]*

Material Preparation

Basal- and edge-oriented HOPG electrodes were purchased from Pine Research and were polished and washed prior to characterizations and HzOR testing. Graphite powder was purchased from Fisher Chemical, and rGO from ACS Materials, both used without further modifications. To prepare ball-milled graphite, 3 g graphite powder was put in a ZrO_2 cell, with 54 ZrO_2 balls. Then, the cell was filled with Ar, tightly sealed with Teflon tape, and milled in a Retsch Crymill for 7 hours at 30 Hz. The control sample ball-milled graphite-HCl, ball-milled graphite was stirred with 32% HCl for 24 hours, filtered and washed with copious amounts of DDI water, then dried in vacuum at 60 °C.

Material characterization

Characterization was performed using powder X-ray diffraction (XRD, Rikagu SmartLab), high-resolution scanning electron microscopy (HRSEM, Zeiss-ultra+, 3 kV), high-resolution transmission electron microscopy (HRTEM, FEI Tecnai, 200 kV), X-ray photoelectron spectroscopy (XPS, UHV ~ $2{\cdot}10^{-10}$ torr using a Versa-probe III, PHI Instruments, 100 mm beam size, energy pass = 224 eV, step size = 0.4 eV, dwell time = 20 ms). ICP-MS used a CHN analyzer of the brand Elementar model Vario Mikro Cube. Chlorine was determined with an ion chromatography of the brand Metrohm Model 883 Plus after a combustion digestion.

Electrochemical procedures

Electrocatalytic hydrazine oxidation (HzOR) experiments were performed at room temperature in a three-electrode cell connected to a bipotentiostat (BioLogic 600). Catalyst-coated glassy carbon electrode (GCE), a graphite rod and a standard calomel electrode (SCE) were used as working, counter and reference electrodes, respectively. Before each run, the SCE was measured against a master electrode, to receive its present potential. For the catalyst ink, 2.5 mg of the sample (or 0.5 mg of rGO) was dispersed in a mixture of 90 µL ethanol, 150 µL of DI water and 10 µL of Nafion solution in IPA (0.5 wt%) and sonicated for 30 minutes. 10 µL of the ink were deposited on a freshly polished GCE (A = 0.196 cm^2) and dried at 50 °C in air. The mass loading on the working electrode was 0.1 mg (0.02 mg for rGO). In addition, highly oriented pyrolytic graphite (HOPG, A = 0.114 cm^2) electrodes were polished to remove impurities and washed with water. N_2-purged 1 M KOH (pH = 14) electrolyte solutions employed for HzOR experiments. Cyclic voltammetry was carried at a potential range from –0.9 to 0.1 V (vs. SCE) for HzOR experiments, and prior to N_2H_4 addition, a wetting sequence was performed by cycling the electrodes in the forementioned potentials.
Electrochemical active surface area (ECSA) measurements were performed from the double layer capacitance of the materials. The capacitance was determined from the CV cycles at 8 scan rates (5, 10, 20, 50, 100, 250 mV s^{-1}) at a small potential window of -0.2 V to 0 V (vs. SCE) in 1 M KOH, N_2-purged solutions, where no Faradaic processes are occurring. The following equation was used:

$$A_{ECSA} = \frac{Double\ layer\ capacitance}{40\ \mu F\ cm^{-2}}$$

this calculation assumes a typical value of 40 mF cm^{-2} for the surface-area normalized capacitance associated with double-layer charging.[1]

Types of Carbon Binding States by XPS C 1s Deconvolution

Table S1. Data summary of atomic percentages from XPS C 1s spectra deconvolution.

Material	C_g (at%)	C-C (at%)	C-OH (at%)	C-O-C (at%)	C=O (at%)	O-C=O (at%)
Graphite	85.98	0.00	0.00	2.07	1.36	1.42
rGO	78.36	0.00	4.57	2.99	1.97	1.87
Ball-milled graphite	82.33	0.00	0.28	2.44	2.56	1.22

Elemental Analysis of Carbons by ICP-MS

Table S2. Atomic percentages of different elements from ICP-MS analysis.

Material	C% (at%)	H% (at%)	N% (at%)	Fe% (at%)	Cl% (at%)	S% (at%)	O% (at%)
Graphite	99	0.71	0.01	0.01	0	0	0.27
rGO	99.13	0.83	0.02	0	0	0	0.03
Ball-milled graphite	94.28	5.58	0	0.09	0.04	0	0.01
Ball-milled graphite HCl	96.07	3.58	0.00	0.00	0.03	0.01	0.31

Additional Micrographs

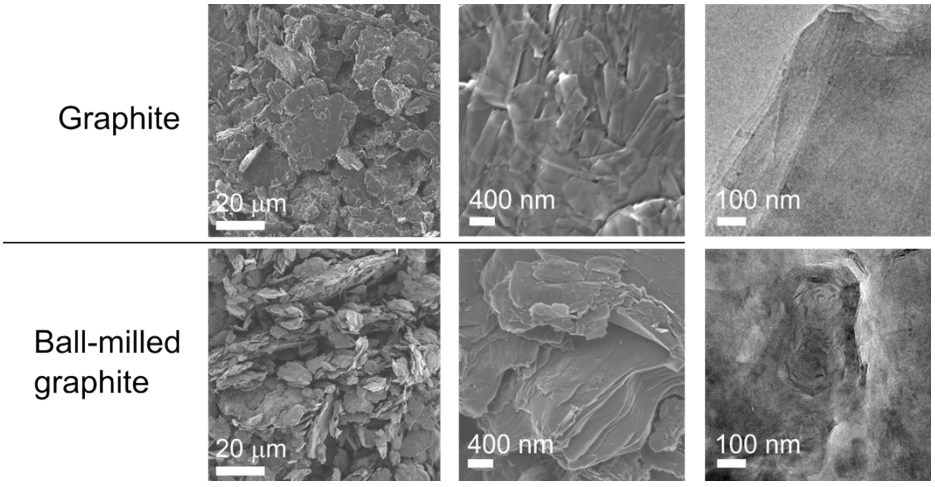

Figure S1. Additional SEM and HRTEM micrographs of graphite and ball-milled graphite, showing breaking of the graphite by the ball-mill treatment.

Reduced graphene oxide (rGO) Characterizations

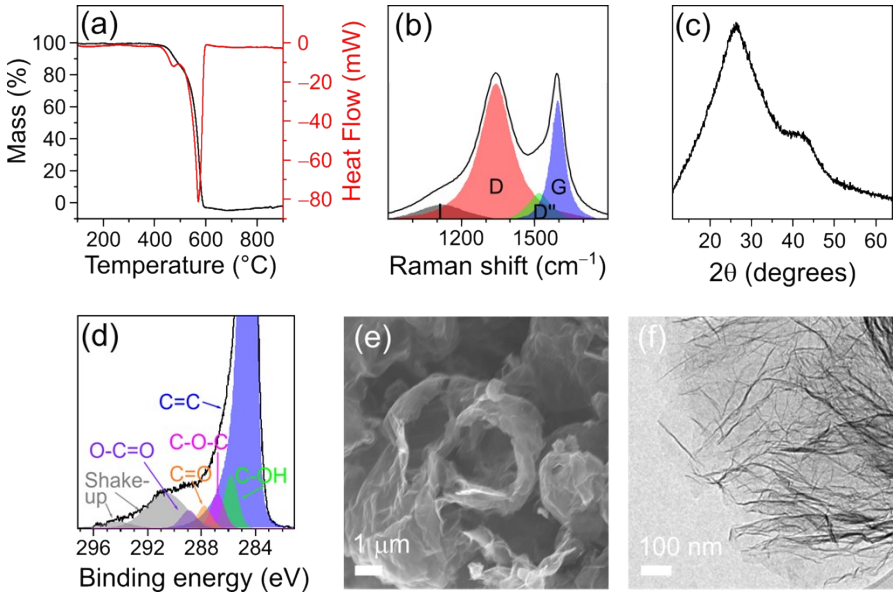

Figure S2. (a) TGA-DSC of rGO in 20% O_2 /80% Ar mixture, 60 ml/minute flow rate. (b) Deconvoluted Raman spectrum. (c) XRD diffractogram. (d) Deconvoluted XPS C 1s spectrum, with assigned peaks. (e) SEM and (f) TEM micrographs. Although the Raman and XPS C 1s spectra may give the impression that rGO has a higher density of edge defects compared to graphite and ball-milled graphite, due to the prominent Raman D band and XPS C_xO_y peaks, this actually arises from the residual graphene oxide (as identified by TGA-DSC, Figure S2a). Moreover, the crumpled morphology of rGO causes the interaction volume of the Raman/XPS beam to accommodate more edges of the perimeters, in relation to the basal-positioned carbon atoms (visualized in Scheme S1).

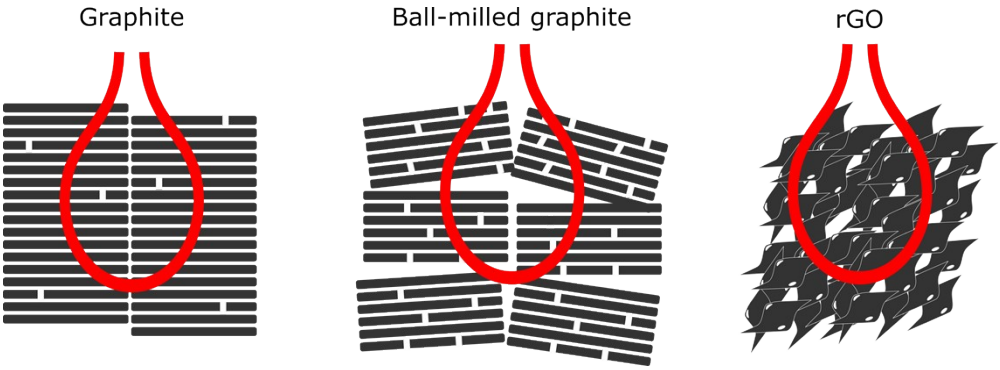

Scheme S1. Illustration of the photon beam interaction volume (red) with basal planes and edge/defect sites in graphite, ball-milled graphite and rGO. The morphology of the rGO leads to the interaction volume to encompass a larger fraction of edges, compared to graphite and ball-milled graphite.

Electrochemical Surface Area

Table S3. Electrochemical surface area (ECSA) of carbon materials.

Material	ECSA (m^2 g^{-1})
rGO	70.5
Graphite	6.3
Ball-milled graphite	9.2
Ball-milled graphite-HCl	9.9

HzOR Activity of Ball-Milled Graphite Before and After HCl wash

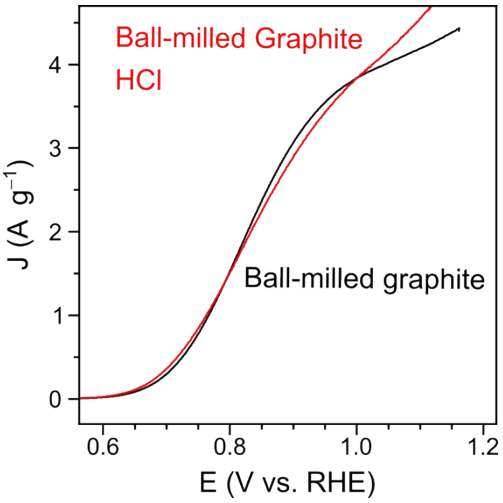

Figure S3. HzOR LSV comparison of ball-milled graphite before and after HCl treatment. 1M KOH, 10 mV s^{-1}, 20 mM N_2H_4.

DFT Calculations Methods

DFT calculations were performed using the Gaussian 09 package. All calculations were carried out with 6-311++g** basis set with Perdew-Burke-Ernzerhof (PBE) functional for optimization of the geometries. Frequency calculations confirmed that the optimized structures were indeed minima or saddle points. We propose an alternate mechanism for the start of the HzOR, and the following processes were used in this work for calculating the reaction Gibbs free energies:[2,3]

$$N_2H_4 \rightarrow N_2H_3^* + H^* \text{ (adsorption)}$$

$$N_2H_3^* + H^* \rightarrow N_2H_3^* + H^+ + e^- \quad (1)$$

$$N_2H_3^* \rightarrow N_2H_2^* + H^+ + e^- \quad (2)$$

$$N_2H_2^* \rightarrow N_2H^* + H^+ + e^- \quad (3)$$

$$N_2H^* \rightarrow N_2^* + H^+ + e^- \quad (4)$$

$$N_2^* \rightarrow N_2 \text{ (desorption)}$$

The first step here corresponds to the adsorption of N_2H_4 such that a N-H bond is simultaneously broken as the N_2H_3 and H species get adsorbed on vicinal carbon atoms. The following steps are the same as the typical hydrazine oxidation mechanism.

Table S4. Minimum ΔG_{max} values for HzOR on different graphitic defects, with smaller values pointing to more active sites.

Defect site	ΔG_{max} (eV)
Pentagon	12.42
Hole	0.94
Armchair	1.46
ZigZag	1.88
Unsat Armchair	0.76
2 Unsat Armchair	0.67
OH Armchair	2.75
Unsat Zagzag	0.78

Explaining the 'Double Peak' Phenomenon in HzOR on Carbon

Table S5. Comparison of the position of the second HzOR catalytic peak in doped-carbon catalysts with reduced graphene oxide peak. Reports which fulfilled the following criteria were selected: (1) carbon-supported catalysts, (2) voltammograms are in potential ranges extended to 1 V vs. RHE and beyond. (3) A pH = 14 electrolyte solution, as used in our work, since changing the concentration of OH^- alters the HzOR catalytically, regardless of the catalyst. All voltammograms show a peak or a rise close to 1 V vs. RHE, even when a control carbon catalyst, absent of the main active site, is applied.

Material	Second HzOR Peak/Rise (V vs. RHE)	Reference
Reduced graphene oxide (rGO)	0.99	This work
Fe-, N-doped carbon (Wash-NC_{Fe})	1.00	[4]
N-, Fe-, Mo-doped carbon (Wash-Fe_2MoC)	1.05	[5]
N-doped carbon (C700)	1.00	[6]
Se-, N-doped carbon (SeNCM-1000)	0.97	[7]
Fe-doped carbon (Fe/C)	0.95	[8]
Co-, W-doped carbon (Co_6W_6C@C)	1.00	[9]

References

1 C. Tang, W. Wang, A. Sun, C. Qi, D. Zhang, Z. Wu and D. Wang, *ACS Catal.*, 2015, **5**, 6956–6963.
2 Y. Zheng, F. He, M. Chen, J. Zhang, G. Hu, D. Ma, J. Guo, H. Fan, W. Li and X. Hu, *ACS Appl. Mater. Interfaces*, 2020, **12**, 38183–38191.
3 Y.-C. Wang, L.-Y. Wan, P.-X. Cui, L. Tong, Y.-Q. Ke, T. Sheng, M. Zhang, S.-H. Sun, H.-W. Liang, Y.-S. Wang, K. Zaghib, H. Wang, Z.-Y. Zhou and J. Yuan, *Small*, 2020, **n/a**, 2002203.
4 J. A. Varnell, J. S. Sotiropoulos, T. M. Brown, K. Subedi, R. T. Haasch, C. E. Schulz and A. A. Gewirth, *ACS Energy Lett.*, 2018, **3**, 823–828.
5 K. Ojha, E. M. Farber, T. Y. Burshtein and D. Eisenberg, *Angew. Chem. Int. Ed.*, 2018, **57**, 17168–17172.
6 E. M. Farber, K. Ojha, T. Y. Burshtein and D. Eisenberg, *J. Electrochem. Soc.*, 2020, **167**, 064517.
7 T. Wang, Q. Wang, Y. Wang, Y. Da, W. Zhou, Y. Shao, D. Li, S. Zhan, J. Yuan and H. Wang, *Angew. Chem.*, 2019, **131**, 13600–13605.
8 J. Zhang, Y. Wang, C. Yang, S. Chen, Z. Li, Y. Cheng, H. Wang, Y. Xiang, S. Lu and S. Wang, *Nano Res.*, DOI:10.1007/s12274-021-3397-9.
9 C. Zhang, M. Zhang, J. Zhu, B. Liu, Y. Hou, J. Wang and J. Niu, *Chem. Commun.*, DOI:10.1039/D1CC03446D.